



# A multi-parameter discrimination digital positron annihilation lifetime spectrometer using a fast digital oscilloscope

Q.H. Zhao<sup>a</sup>, R. Ye<sup>a</sup>, H.B. Wang<sup>a</sup>, L.H. Cong<sup>a</sup>, J.D. Liu<sup>a</sup>, H.J. Zhang<sup>a,b,\*</sup>, B.J. Ye<sup>a,b,\*</sup>

<sup>a</sup> State Key Laboratory of Particle Detection and Electronics, University of Science and Technology of China, Hefei 230026, China

<sup>b</sup> Hefei National Laboratory for Physical Sciences at the Microscale, University of Science and Technology of China, Hefei 230026, China

## ARTICLE INFO

### Keywords:

Positron annihilation lifetime spectrometer  
Data processing methods  
BaF<sub>2</sub>  
Timing detectors  
Pulse discrimination

## ABSTRACT

Positron annihilation lifetime (PAL) spectroscopy is widely used in the characterization of material microstructures. It has a very high sensitivity to the material defects. This paper describes how we developed a digital PAL spectrometer with two barium fluoride (BaF<sub>2</sub>) detectors and reading the data with a fast digital oscilloscope. We achieved better time performance for the digital PAL spectrometer using a multi-parameter discrimination method and various pulse smoothing algorithms. With two BaF<sub>2</sub> detectors in the coincidence mode, we achieved a time resolution of 160 ps for 0.511 MeV annihilation gamma rays. The multi-parameter discrimination method implemented can remove incorrect events more effectively than the conventional energy discrimination method. With this enhancement in event discrimination, the digital PAL spectrometer's time performance has improved, which results in more accurate PAL characterization. In a lifetime measurement, the PAL spectrometer's time resolution is about 130 ps, which is much better than most PAL spectrometers. With the multi-parameter discrimination method, the resolution component from the incorrect events decreases drastically, and the leading edge distortion of the PAL spectrum is significantly improved.

## 1. Introduction

Positron annihilation lifetime (PAL) spectroscopy has become an important means to study the microstructures of materials. It is very sensitive to defects in solids [1–3]. A conventional analog PAL spectrometer consists of a pair of scintillation detectors, two constant fraction differential discriminators (CFDD), a time-to-amplitude converter (TAC), and a multichannel analyzer (MCA). Its analog electronics limit the time resolution of a conventional analog PAL spectrometer. As the analog PAL spectrometer only performs simple discrimination of the pulse energy, the improvement of accuracy requires more complex devices [4,5].

With the development of waveform digitization technology, several digital PAL spectrometers have been developed by substituting the analog electric modules with a digital oscilloscope or fast digitizers [6–11]. This technology can obtain the complete waveform of the signals, and can ensure that the signals have almost no distortion. The original signal data can ensure that the information is accurate. Pulse smoothing algorithm can make timing more accurate and reduce the influence of white noise. Therefore, the PAL spectrometers' time performance can be effectively improved by applying various timing algorithms on the signal waveforms. Several digital PAL spectrometers with high time resolution have been developed due to such improvement [6, 10,12,13]. The waveform digitization technology makes it possible to

use several discrimination methods besides the energy discrimination methods [7,10,13,14], resulting in more accurate PAL characterization experiments.

In this work, a digital PAL spectrometer was developed using two BaF<sub>2</sub>-coupled PMT detectors and a digital oscilloscope (LeCroy HDO 9204). A variety of pulse smoothing algorithms were used to improve the time performance of the digital PAL spectrometer. Two timing methods were compared in the measurements [15]. Multi-parameter discrimination reduce interference caused by incorrect events. In lifetime measurement, the PAL spectrometer's time resolution is about 130 ps, the intensity of the resolution component from the false events decreases significantly by using the multi-parameter discrimination method, leading edge distortion of the PAL spectrum is improved substantially.

## 2. Experimental setup and analysis method

The detectors were BaF<sub>2</sub> scintillators coupled to photomultiplier tubes (PMT) (H6610, from Hamamatsu) with silicon grease. Teflon tape wrapped the BaF<sub>2</sub> scintillators (from Beijing Scitlion Technology Corp., Ltd.). The dimensions of the scintillators are  $\Phi 20 \times 15$  mm. The operating voltage of the PMTs was  $-2500$  V. This experiment used a <sup>22</sup>Na source with an activity of 30  $\mu$ Ci, and the counting rate

\* Corresponding authors.

E-mail addresses: [hjzhang8@ustc.edu.cn](mailto:hjzhang8@ustc.edu.cn) (H.J. Zhang), [bjye@ustc.edu.cn](mailto:bjye@ustc.edu.cn) (B.J. Ye).

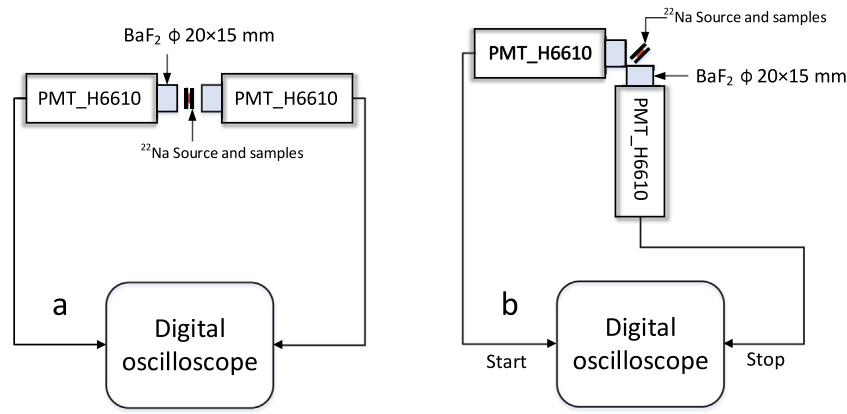


Fig. 1. Schematics of PAL spectrometer setups for (a) coincidence time resolution (CTR) measurements and (b) lifetime measurements.

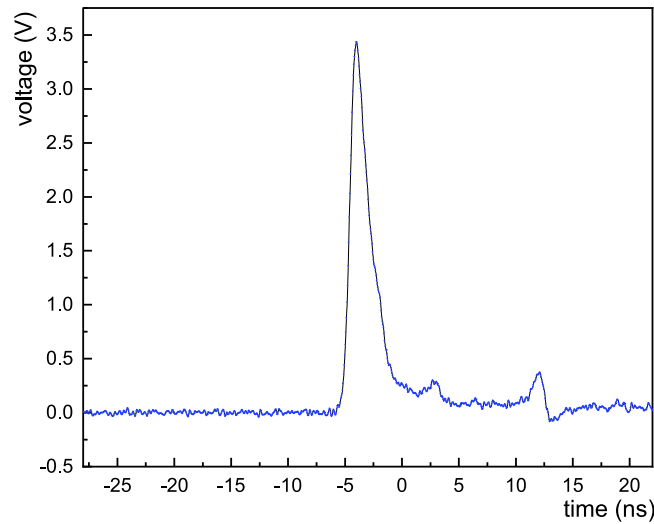


Fig. 2. The signal from the anode of the start detector. Negative pulses are converted to positive pulses for using in data processing program.

was about 70 cps in lifetime measurement. The experiment used two yttria-stabilized zirconia samples (YSZ) to test the PAL spectrometer's performance.

Fig. 1 shows the schematic diagrams of the PAL spectrometer, which consists of two detectors and a digital oscilloscope. The figure also shows that the sensors have two different geometries. One geometry is used for coincidence time resolution (CTR) measurements, and the other is for lifetime measurements. A 1.275 MeV nuclear  $\gamma$ -ray is emitted simultaneously with a positron from  $^{22}\text{Na}$  and is the start signal in lifetime measurement. The two 0.511 MeV annihilation  $\gamma$ -rays that are emitted back-to-back are the stop signal. The PAL spectrometer setup in Fig. 1(b) can reduce signal pile-up in the start detector (when the start detector detects the 0.511 MeV  $\gamma$ -ray and the 1.275 MeV  $\gamma$ -ray simultaneously) so that the distortion of PAL spectra can be minimized [5,16]. The digital oscilloscope recorded the anode pulses of the detectors in ch1 and ch3. A qualified triggering mode triggered the digital oscilloscope once both two input signals reached the threshold within a restricted time window. If the triggering condition is satisfied in one event, the signals are digitized into discrete waveform data and saved in the hard disk. Data analysis was done offline. The offline software was written in C++ and used the GNU Scientific Library (GSL) [17] and ROOT [18], our code could be download on GitHub [19].

Fig. 2 shows a signal from the start detector. As the detector's anode signals are negative and our program can only handle the positive pulses, the anode signals were converted to positive pulses. The rise

time of the pulses is 1 ns. The waveform data were acquired by the oscilloscope operating at a sampling rate of 20 Gs/s and a sampling time interval of 50 ps. The time window of input channels is 50 ns.

## 2.1. Timing analysis

Time resolution is one of the most critical parameters of a PAL spectrometer. We used two different timing methods and compared them to achieve the best resolution. They are the leading-edge digital timing (DLET) method and the digital constant fraction timing (DCFT) method. The "arrival time" of a signal obtained by the DLET method is set when the amplitude is over a voltage threshold. The principle of the DCFT is different. A time stamp is created at the constant fraction level of the signal amplitude. During the data processing, the waveform data is first smoothed. Then, the smoothed waveform can be timed by the DLET method ( $t_{DLET}$ ) or the DCFT method ( $t_{DCFT}$ ). The smoothing algorithms are shown in the following.

### 2.1.1. Linear interpolation

Linear interpolation is the most common method to smooth the curve between two points. By connecting straight lines between adjacent points, the time of the trigger is determined. The points that are adjacent to the threshold ( $V_{level}$ ) are defined as ( $t_0, V_0$ ) and ( $t_1, V_1$ ). The time-mark  $t_{mark}$  can be calculated by

$$t_{mark} = (V_{level} - V_0) * \frac{t_1 - t_0}{V_1 - V_0} + V_0 \quad (1)$$

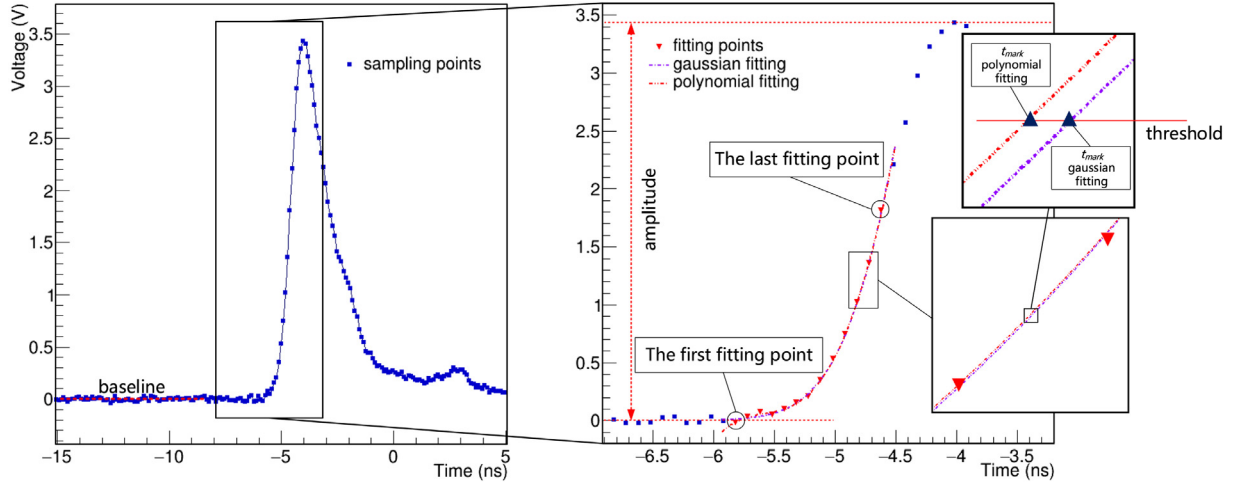


Fig. 3. A schematic of the fitting method. The first fitting point is the last point below the baseline. It is the start of the pulse. The last fitting point is the first point over a fixed fraction (50% in this figure) of the amplitude.

### 2.1.2. Polynomial fitting

A polynomial can approximate any curve, so high-order polynomials were used to fit the signal's leading edge to smooth the data. GSL provided the polynomial fitting function. Third to fifth-order polynomials were used to fit the waveform data. The fitting range was from the start point (the last point below the baseline) of the pulse to the first point over a fixed fraction (40%, 50%, 60%) of the amplitude. The schematic of the fitting method is shown in Fig. 3. After fitting the curve, the  $t_{mark}$  can be calculated.

### 2.1.3. Spline interpolation

Spline interpolation is a form of interpolation which uses a polynomial. The polynomial curve is called a spline. Spline interpolation is often preferred over polynomial interpolation because the interpolation error can be small even when using a low degree polynomial for the spline [20]. The interpolation curve between sampling points ( $q_1, q_2, \dots, q_n$ ) must meet the following conditions:

$$\begin{cases} q'_i(t_i) = q'_{i+1}(t_i) \\ q''_i(t_i) = q''_{i+1}(t_i) \end{cases} \quad 1 \leq i \leq n-1 \quad (2)$$

GSL provided the spline interpolation function, Cubic spline was used in this work. The interpolation function returns the curve as discrete points, so we insert nine points between every two sampling points and linearly interpolate them again to obtain better results.

### 2.1.4. Gaussian fitting

The Gaussian fitting is used widely in others' work [7–9], because the left pulse edge exhibits Gaussian shape, can be more correctly described with a Log-Normal form [21]. We used Gaussian function to fit the pulse edge. The Gaussian fitting function from ROOT is used. The fitting range is the same as the one used for the polynomial fit. After fitting the curve, the  $t_{mark}$  can be calculated.

## 2.2. Discrimination method

Pulse discrimination is obtained by filtering the waveform data. We used energy discrimination to distinguish the start signal (1.275 MeV) and the stop signal (0.511 MeV) in the lifetime measurement. With the development of waveform digitization technology, pulse discrimination methods have become diverse, and are no longer limited to energy discrimination. Correlating the pulse amplitude with the pulse area can remove outliers in a two-dimensional space and make the discrimination more effective [22]. We studied the relationship between pulse amplitude and area, and the relationship between rise time and pulse width. Some mathematical methods were used to reduce the

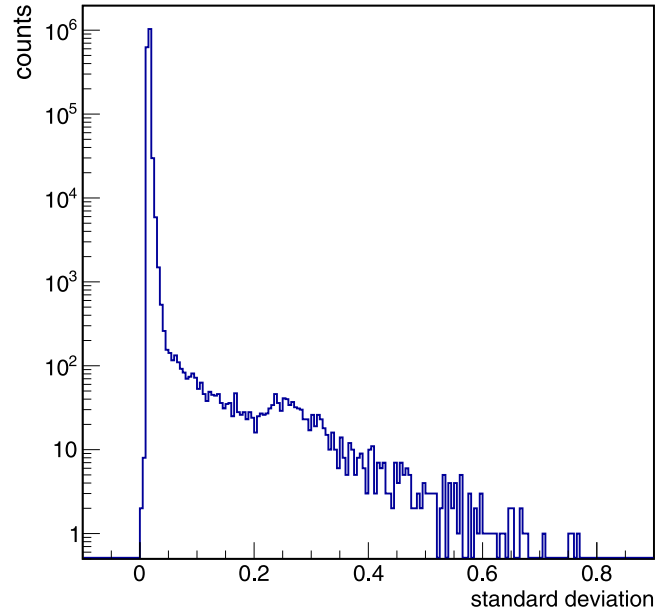


Fig. 4. The distribution of the standard deviation of the sampling points' values at the baseline.

dimensionality of the two-dimensional data, making the discrimination more intuitive and effective. A variety of discrimination methods are shown in the following.

### 2.2.1. Correction of the baseline-offset and baseline discrimination

As baseline drift creates inaccurate data analysis, a digital baseline correction was used to eliminate its effects. We selected 50 sampling points before the pulse and took the average as the baseline-offset value. Before performing other analyses, the baseline-offset was removed from the data. Baseline can also be used for pulse discrimination [22]. We calculated the standard deviation of the sampling points' values at the baseline. The distribution of the standard deviation is shown in Fig. 4. Waveform data with a standard deviation more than 0.2 would be removed.

### 2.2.2. Pulse amplitude and area discrimination

Pulse amplitude and pulse area (integral) can be used to measure energy deposition. In the positron lifetime measurement, pulse area

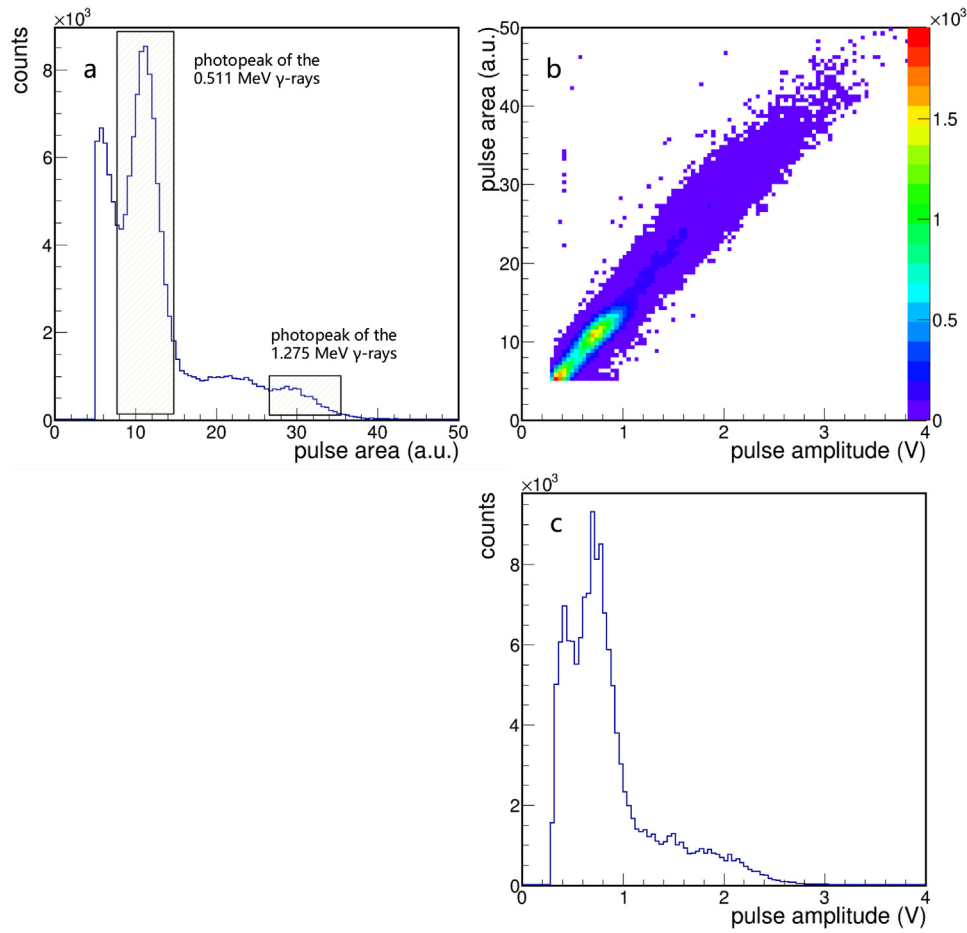


Fig. 5. Insert (a) shows a pulse spectrum and insert (c) shows an amplitude spectrum. Insert (b) shows a amplitude-area 2-D histogram.

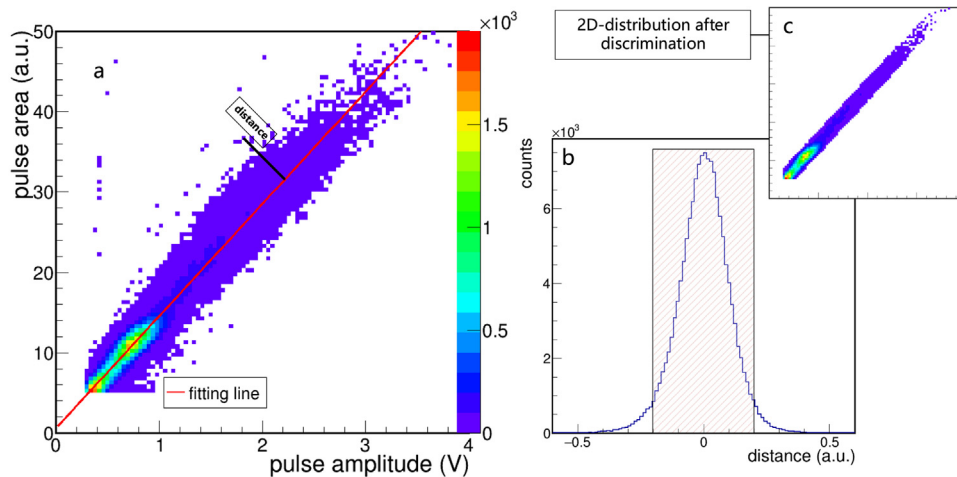


Fig. 6. The schematic of pulse amplitude-area discrimination with a linear fit. Insert (b) shows the distance distribution to that fitted line. Events whose absolute distance is greater than 0.2 are eliminated and the 2D pulse amplitude-area plot after this discrimination process is shown in insert (c).

discrimination was used as a method to distinguish the 1.275 MeV  $\gamma$  (start signal) and 0.511 MeV  $\gamma$  (stop signal). Fig. 5(a) and (c) show the pulse area spectrum and the amplitude spectrum of the <sup>22</sup>Na source. These plots can all be used for energy discrimination. The area spectrum has a more meaningful energy calibration than the amplitude spectrum. Therefore, we used the area spectrum to distinguish the start signal (from 26 to 35) and the stop signal (from 8 to 15).

A pulse amplitude-area 2-D histogram is shown in Fig. 5(b). There is a clear linear relationship between the amplitude and the area. Most

of the data is concentrated around a straight line. There are a few outliers that need to be eliminated. We fit the pulse amplitude and the pulse area linear (Fig. 6(a)) and calculated the distance from each point (amplitude, area) to the fitted line. Points above the fitted line are set to a negative distance. The distance distribution is shown in Fig. 6(b). The discrete data points in which the absolute value of the distance is more than 0.2 are eliminated. The pulse amplitude-area 2-D histogram after discrimination is shown in Fig. 6(c).

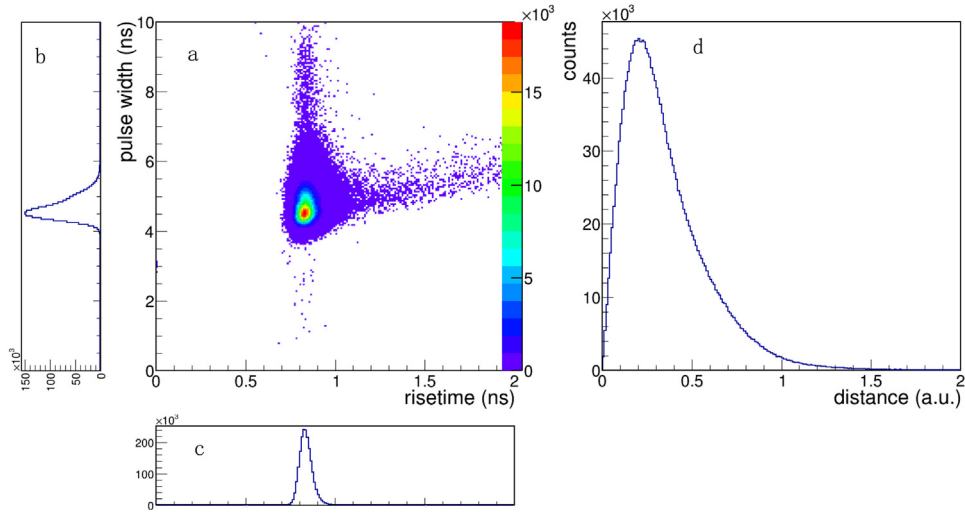


Fig. 7. The pulse rise time and width 2-D histogram and the pulse rise time, the pulse width and the weighted distance ( $D_{weight}$ ) histograms.

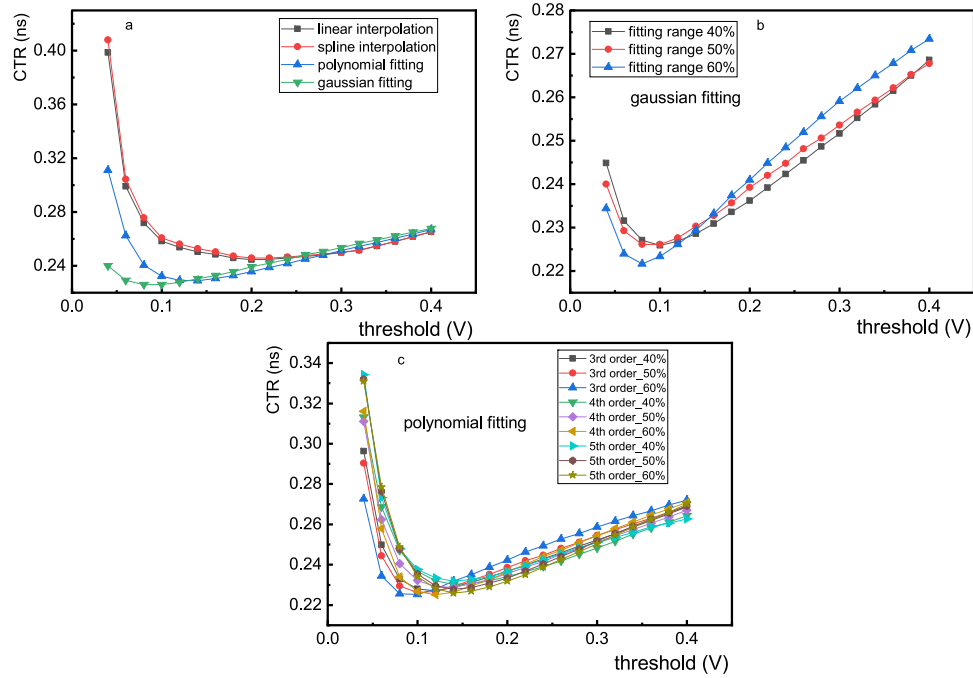


Fig. 8. Variations of CTR as a function of timing threshold for different pulse smoothing algorithms with the DLET method. The difference between algorithms is shown in insert (a). In insert (b), different curves represent different fitting ranges with a Gaussian fit. In insert (c), a variety of polynomial orders and fitting ranges are considered.

### 2.2.3. Pulse rise time and width discrimination

Pulse rise time is defined as the interval of time required for a pulse to rise from 10% to 90% of the peak pulse amplitude. Pulse width is defined as the interval of time that the pulse exceeds 10% of the peak pulse amplitude. The pulse rise time and width are determined by the performance of PMT and the rise time and decay time of the pulse produced in the scintillator. However, the  $\gamma$ -ray interactions in the scintillation region and near the detector's dead region may contribute to pulse distortion. This effect leads to pulses with a longer rise time or longer width [23]. A pulse rise time and width 2-D histogram is shown in Fig. 7(a).

First, we find the maximum density point  $P_{max}$  ( $P_{risetime}$ ,  $P_{width}$ ) in the 2-D histogram. The histogram is divided into 10000 pixels. The center of the pixel which has the most points is considered the maximum density point. Then, we calculate the weighted distance ( $D_{weight}$ ) from each point ( $r$ ,  $w$ ) to  $P_{max}$ . The weighted distance ( $D_{weight}$ )

is calculated by

$$D_{weight} = \sqrt{\left(\frac{r - P_{risetime}}{w_{pr}}\right)^2 + \left(\frac{w - P_{width}}{w_{pw}}\right)^2} \quad (3)$$

$w_{pr}$  and  $w_{pw}$  are the full width at tenth maximum (FWTM) of the pulse rise time and width distributions as shown in Fig. 7(b) and (c). The  $D_{weight}$  distribution is shown in Fig. 7(d). The pulse rise time and width discrimination window is based on  $D_{weight}$ . The primary motivation for creating this window is to filter out the pulses with longer pulse rise times and pulse widths.

### 3. Results and discussion

Different timing methods and smoothing algorithms were tested for the CTR measurement. As shown in Fig. 1(a), two detectors were placed in face-to-face geometry. A  $^{22}\text{Na}$  source was inserted between the two

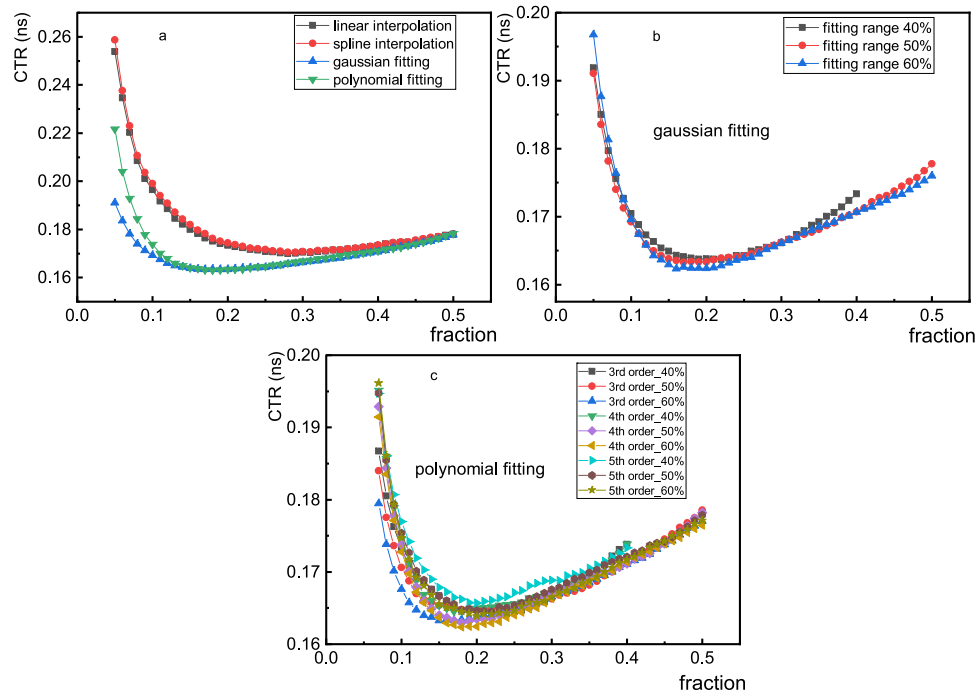


**Fig. 9.** Variations of CTR as a function of timing fraction for different pulse smoothing algorithms with the DCFT method. The difference between algorithms is shown in insert (a). In insert (b), the colored curves represent different fitting ranges with Gaussian fitting. In insert (c), a variety of polynomial orders and fitting ranges are shown. (For interpretation of the references to color in this figure legend, the reader is referred to the web version of this article.)

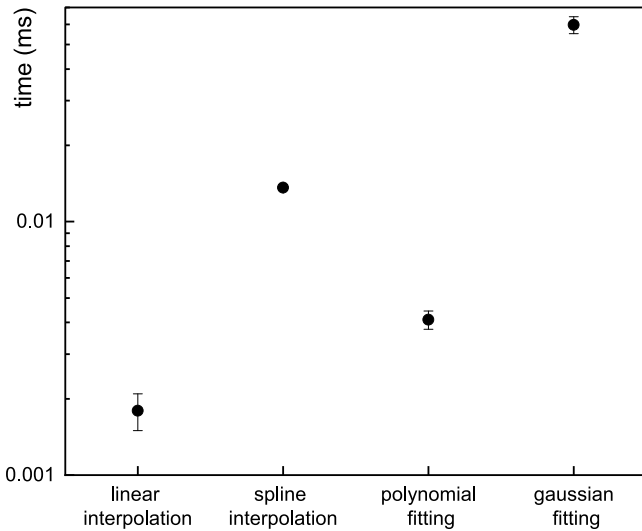


**Fig. 10.** The processing time for 100 groups of waveform data with different algorithms. Intel(R) Core(TM) i3-3240 @3.40 GHz, Ubuntu 16.04.

detectors. The CTR measurement measured the time difference between the 0.511 MeV annihilation  $\gamma$ -ray pairs. In such a CTR measurement, different smoothing algorithms and timing methods were used to obtain the optimal time resolution. The CTR values were derived from a Gaussian fit of the time difference between the two 0.511 MeV annihilation  $\gamma$ -rays. The fit results for different smoothing algorithms and timing methods are shown in Figs. 8 and 9.

The influence of different smoothing algorithms and thresholds on the CTR for DLET is shown in Fig. 8. To find the optimum DLET threshold, we varied the threshold from 40 to 400 mV in steps of 20 mV. Regardless of the algorithm, the leading-edge timing's timing threshold has the same effect on the time resolution. As the timing threshold increases, the CTR will first decrease and then increase.

The results of the two interpolation algorithms are similar. The best CTR and corresponding timing threshold are [244.49 ps, 200 mV] (linear interpolation) and [245.76 ps, 220 mV] (spline interpolation). The fitting algorithms are significantly better than the interpolation algorithms. For Gaussian fitting, 60% fitting range provides the best performance with [221.61 ps, 80 mV]. For polynomial fitting, the best combination is a fourth-degree polynomial fit and a 60% fitting range. The best CTR and corresponding timing threshold are [225.16 ps, 120 mV]. The results of the fitting algorithms are better than that of the interpolation algorithm because the fitting algorithms can reduce the white noise's influence on the signal's leading edge.

The results of the CTR measurements with DCFT are shown in Fig. 9. Different constant fraction values were used to find the best timing performance. For different smoothing algorithms, the timing constant fraction value has the same effect on the time resolution. As the fraction value increases, the CTR first decreased and then increased. The results of the two interpolation algorithms are similar. The best CTR and corresponding fraction of interpolation algorithms are [169.98 ps, 0.28] (linear interpolation) and [170.46 ps, 0.29] (spline interpolation). For Gaussian fitting, the best of the three fitting ranges is 60%, and the best CTR and corresponding fraction is [162.38 ps, 0.2]. For polynomial fitting, the best combination is the fourth-degree polynomial fitting and 60% fitting range, and the best CTR and corresponding fraction are [162.35 ps, 0.18].

The best CTRs of different smoothing algorithms and timing methods are listed in Table 1. The results of DCFT are much better than DLET. Whether it is DCFT or DLET, the fitting algorithms are better than interpolation algorithms. The results of Gaussian fitting are similar to polynomial fitting. Considering the calculation time (Fig. 10), DCFT and polynomial fitting are the best combination to get the best time resolution.

Positron annihilation lifetime spectra for YSZ samples were measured to investigate the performance of the digital PAL spectrometer. The 9 mol %  $Y_2O_3$  doped YSZ samples (from Hefei Kejing Materials Technology Co., Ltd.) were used as reference samples for their single positron lifetime component of 180 ps [24,25]. Our digital PAL

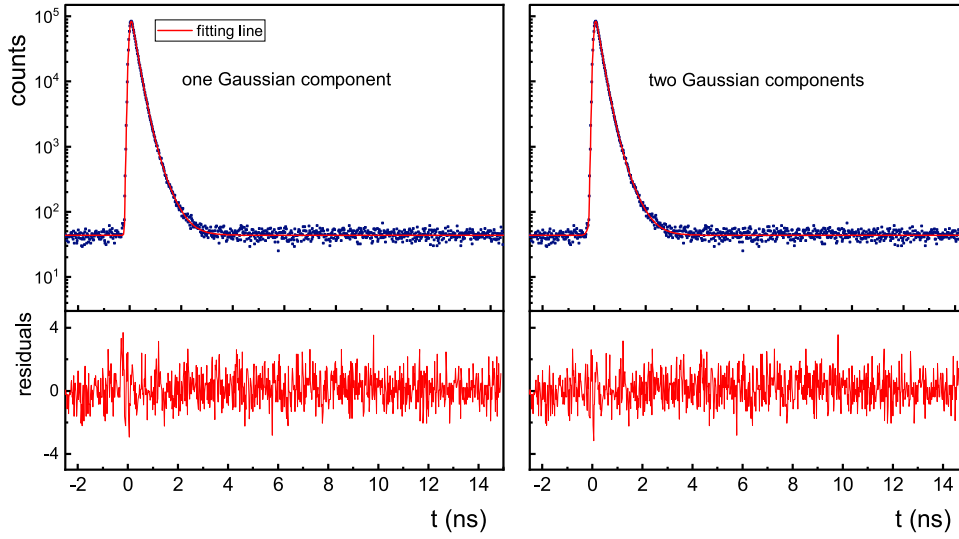


Fig. 11. PAL spectrum of YSZ which was measured by digital PAL spectrometer with multi-parameter discrimination (PAL#1). The left one used a resolution function consisting of one Gaussian component. The right one used resolution function consisting of two Gaussian components.

**Table 1**  
The best CTRs of different smoothing algorithms and timing methods.

Timing method	Smoothing algorithm	Coincidence time resolution (ps)	Threshold (mV)
DLET	Linear interpolation	244.49±1.35	200
	Spline interpolation	245.76±1.41	220
	Gaussian fitting	221.61±1.49	80
	Polynomial fitting	225.16±1.33	120
Timing method	Smoothing algorithm	Coincidence time resolution (ps)	Fraction
DCFT	Linear interpolation	169.98±0.93	0.28
	Spline interpolation	170.46±0.92	0.29
	Gaussian fitting	162.38±1.02	0.2
	Polynomial fitting	162.35±0.93	0.18

**Table 2**  
Analysis results of PAL spectra of YSZ with one Gaussian component, PAL#1 is collected by digital PAL spectrometer with multi-parameter discrimination, and PAL#2 is collected by digital PAL spectrometer without multi-parameter discrimination. PAL#3 comes from analog PAL spectrometer.

	PAL#1	PAL#2	PAL#3
$\tau_1$ (ps)	177.89±0.69	178.64±0.50	182.08±0.57
$I_1$ (%)	86.36±0.50	86.71±0.26	90.25±0.29
$\tau_2$ (ps)	398.2±6.0	402.7±2.7	442.3±5.3
$I_2$ (%)	13.64±0.50	13.29±0.26	9.75±0.29
FWHM (ps)	129.6	133.1	183.0
Fit's variance	1.02	1.19	1.61

spectrometer collected two PAL spectra. One used multi-parameter discrimination (PAL#1) and the other only used pulse area discrimination (PAL#2). A total of  $1.4 \times 10^6$  counts were collected for each spectrum. A PAL spectrum was collected by a conventional analog PAL spectrometer, which consists of two detectors (the same as our digital PAL spectrometer) and NIM standard electronic modules (from ORTEC). This spectrum is used as a reference (PAL#3). All spectra were analyzed by the LTV9 program [26], which uses the Gauss-Newton non-linear fitting routines.

A PAL spectrum,  $N(t)$ , which consists of several exponential components convoluted with the time resolution function of the spectrometer [27,28], has the following mathematical form:

$$N(t) = \sum_{i=1}^{k_0} [A_i \exp(-\frac{t}{\tau_i})] \otimes R(t) + B \quad (4)$$

where  $t$ ,  $k_0$ ,  $R$ ,  $B$ ,  $\tau_i$ ,  $A_i$  are the time, number of lifetime components, time resolution function, background, mean lifetime of the  $i$ th lifetime component, and a pre-exponential factor. In most lifetime experiments, the time resolution function  $R(t)$  is usually described as a Gaussian function. In fact, the resolution function of the instrument is complicated and not even symmetric. The resolution function could be described more correctly by a superposition of multiple Gaussians differing by their FWHMs, intensity, and positions [10]. One Gaussian component of  $R(t)$  with a weak intensity and a large FWHM is from the signal distortion caused by pile-up effects, environmental electromagnetic interference. This interference will have an impact on the analysis. Suitable initial fitting values are needed for good fitting results. If we use a quick fit with a single Gaussian component, the results' accuracy cannot be guaranteed. Multi-parameters discrimination can reduce the proportion of error cases. We use two resolution functions to analyze the PAL spectra. The first has one Gaussian component, while the other has two Gaussian components.

Fig. 12 shows the spectrum without multi-parameter discrimination collected by digital PAL spectrometer. The left one used one Gaussian component resolution function, the right one used two Gaussian components. The residuals of the spectrum with one Gaussian component have a small fluctuation on the left. Fig. 11 shows the spectrum with multi-parameter discrimination collected by digital PAL spectrometer. Whether we use one Gaussian component or two Gaussian components resolution function, the spectrum's fitting residuals are evenly distributed in the fitting range. The multi-parameter discrimination can make the PAL spectrometer's resolution function close to a Gaussian function. The reference spectrum collected by an analog PAL spectrometer is shown in Fig. 13. The fitting residuals at the left of the peak fluctuate sharply with one Gaussian component. With two Gaussian components resolution function, the residuals still have some small fluctuations around the peak, so the resolution function should have a more complex composition.

The results of 2 lifetime components fitting of PAL spectra are listed in Tables 2 and 3. The YSZ spectra resulted in two lifetime components  $\tau_1$  and  $\tau_2$ . The shorter lifetime component ( $\tau_1$ ) of around 180 ps is the positron lifetime in the defect-free bulk of the YSZ. The longer lifetime component ( $\tau_2$ ) is from the positron annihilation in  $^{22}\text{Na}$  source and the two source-sealing Kapton foils [29,30]. In the results, which use one Gaussian component resolution function, the FWHM of the spectra measured by the digital PAL spectrometer is around 130 ps, far better than 183 ps of the analog spectrometer. In the results which use two Gaussian components resolution function,

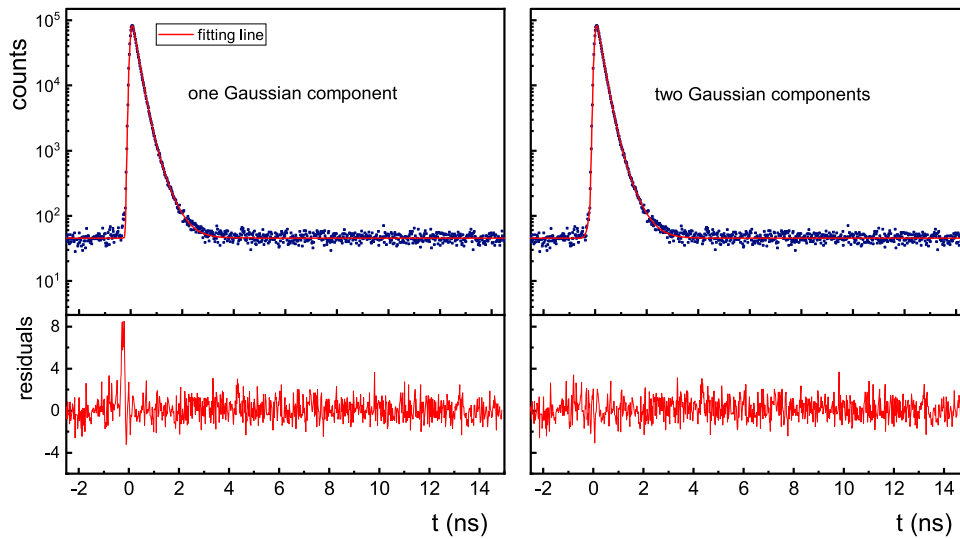


Fig. 12. PAL spectrum of YSZ which was measured by digital PAL spectrometer without multi-parameter discrimination (PAL#2). The left one used a resolution function consisting of one Gaussian component. The right one used resolution function consisting of two Gaussian components.

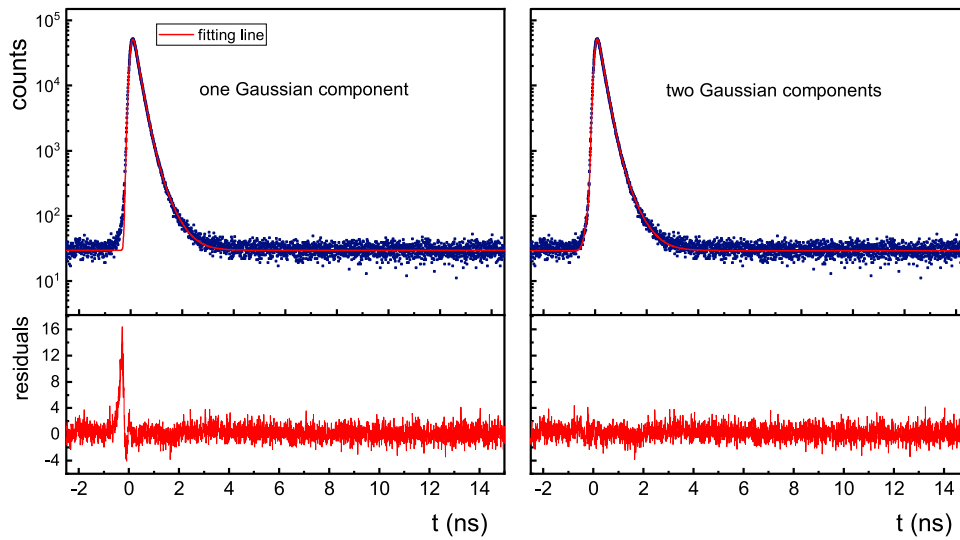


Fig. 13. PAL spectrum of YSZ which was measured by analog PAL spectrometer (PAL#3). The left one used a resolution function consisting of one Gaussian component. The right one used resolution function consisting of two Gaussian components.

the FWHM of the component caused by signal distortion decreases from 371.1 ps to 350.2 ps by using multi-parameter discrimination, and the intensity reduces significantly from 0.73% to 0.22%. Fig. 14(a) shows the resolution function with two Gaussian components. The FWHMs and intensity of the component caused by signal distortion are shown in Fig. 14(b). The fits are excellent with the variation of one resolution component analysis of 1.02, and the variance of the two Gaussian components resolution function analysis is 1.00. By using multi-parameter discrimination, the effect of signal distortion is almost eliminated. By using multi-parameter discrimination, the FWHM of the PAL spectrometer slightly improved from 133.1 ps to 129.6 ps.

#### 4. Conclusions

In this work, a multi-parameter discrimination PAL spectrometer was developed by using BaF<sub>2</sub> scintillators, PMTs, and a digital oscilloscope. The paper compares and then optimizes various pulse smoothing algorithms and timing methods. The digital PAL spectrometer has a good time performance. Among different algorithm parameters, the best CTR value for 0.511 MeV annihilation  $\gamma$ -ray pairs is 162 ps. With

Table 3

Analysis results of PAL spectra of YSZ with two Gaussian components, PAL#1 is collected by digital PAL spectrometer with multi-parameter discrimination, and PAL#2 is collected by digital PAL spectrometer without multi-parameter discrimination. PAL#3 comes from analog PAL spectrometer.

	PAL#1	PAL#2	PAL#3
$\tau_1$ (ps)	178.11±0.53	179.14±0.45	182.96±0.54
$I_1$ (%)	86.52±0.20	87.11±0.20	91.00±0.26
$\tau_2$ (ps)	399.7±2.2	406.9±2.6	455.3±5.4
$I_2$ (%)	13.48±0.20	12.89±0.20	9.00±0.26
FWHM <sub>1</sub> (ps)	129.1	131.3	178.2
$G_1$ (%)	99.7787	99.2693	98.1888
FWHM <sub>2</sub> (ps)	350.2	371.1	476.3
$G_2$ (%)	0.2213	0.7307	1.8112
Fit's variance	1.00	1.02	1.10

the same parameters, the FWHM of the lifetime spectrum is 130 ps. This value is far better than 180 ps, which is found from the analog PAL spectrometer lifetime measurement. By incorporating multi-parameter discrimination, the intensity of the resolution component produced by

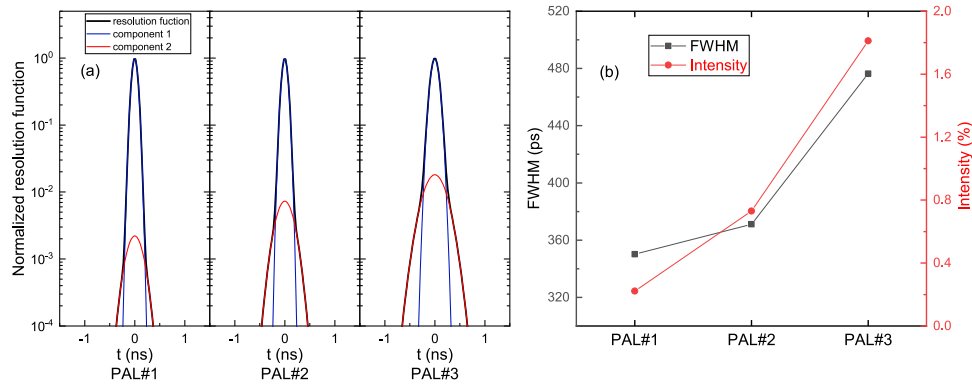


Fig. 14. The resolution functions and corresponding Gaussian components are shown in (a). The FWHM and corresponding intensity of the Gaussian components produced by signal distortion are shown in (b).

signal distortion is reduced from 0.73% to 0.22%. This resolution function is close to ideal. Whether we use the resolution function with one Gaussian component or two Gaussian components, the fitting residuals of the spectrum are evenly distributed in the fitting range. These fit variances are excellent as they are close to 1. Multi-parameter discrimination can effectively eliminate the influence of distortion pulse, make the measurement result more accurate. The time performance of the spectrometer is also improved slightly.

#### CRediT authorship contribution statement

**Q.H. Zhao:** Conceptualization, Software, Formal analysis, Writing – original draft, Visualization. **R. Ye:** Methodology. **H.B. Wang:** Validation. **L.H. Cong:** Validation. **J.D. Liu:** Formal analysis. **H.J. Zhang:** Supervision, Project administration. **B.J. Ye:** Supervision, Project administration, Funding acquisition.

#### Declaration of competing interest

The authors declare that they have no known competing financial interests or personal relationships that could have appeared to influence the work reported in this paper.

#### Acknowledgments

This work was supported by the National Natural Science Foundation of China (Grant Nos. 11775215, 11875248, and 11975225) and the National Key R&D Program of China (Grant No. 2019YFA0210000).

#### References

- [1] P. Hautojärvi, C. Corbel, Positron spectroscopy of defects in metals and semiconductors, in: International School of Physics "Enrico Fermi", Course CXXV, Varenna, Italy, 1993, 1994.
- [2] M. Biasini, Study of the Fermi surface of molybdenum and chromium via positron annihilation experiments, *Physica B* 275 (4) (2000) 285–294, [http://dx.doi.org/10.1016/s0921-4526\(99\)00745-0](http://dx.doi.org/10.1016/s0921-4526(99)00745-0).
- [3] J. Čížek, Characterization of lattice defects in metallic materials by positron annihilation spectroscopy: A review, *J. Mater. Sci. Technol.* 34 (4) (2018) 577–598, <http://dx.doi.org/10.1016/j.jmst.2017.11.050>.
- [4] L. Dorikens-Vanpraet, D. Segers, M. Dorikens, The influence of geometry on the resolution of a positron annihilation lifetime spectrometer, *Appl. Phys.* 23 (2) (1980) 149–152, <http://dx.doi.org/10.1007/bf00899710>.
- [5] L.H. Cong, B.C. Gu, X.X. Han, Q.H. Zhao, Z.W. Pan, R. Ye, J.Q. Guo, B.J. Ye, Reconfigurable positron annihilation lifetime spectrometer utilizing a multi-channel digitizer, *Nucl. Instrum. Methods Phys. Res. A* 946 (2019) 162691, <http://dx.doi.org/10.1016/j.nima.2019.162691>.
- [6] H. Saito, Y. Nagashima, T. Kurihara, T. Hyodo, A new positron lifetime spectrometer using a fast digital oscilloscope and baf<sub>2</sub> scintillators, *Nucl. Instrum. Methods Phys. Res. A* 487 (3) (2002) 612–617, [http://dx.doi.org/10.1016/s0168-9002\(01\)02172-6](http://dx.doi.org/10.1016/s0168-9002(01)02172-6).

- [7] H. Li, Y.D. Shao, K. Zhou, J.B. Pang, Z. Wang, A simplified digital positron lifetime spectrometer based on a fast digital oscilloscope, *Nucl. Instrum. Methods Phys. Res. A* 625 (1) (2011) 29–34, <http://dx.doi.org/10.1016/j.nima.2010.10.005>.
- [8] J. Nissilä, K. Ryttsälä, R. Aavikko, A. Laakso, K. Saarinen, P. Hautojärvi, Performance analysis of a digital positron lifetime spectrometer, *Nucl. Instrum. Methods Phys. Res. A* 538 (1) (2005) 778–789, <http://dx.doi.org/10.1016/j.nima.2004.08.102>, URL <https://www.sciencedirect.com/science/article/pii/S0168900204020005>.
- [9] R. An, B. Chen, Y.F. Liu, B.J. Ye, W. Kong, R. Stefan, A new positron annihilation lifetime spectrometer based on DRS4 waveform digitizing board, *Chin. Phys. C* 38 (5) (2014) 056001, <http://dx.doi.org/10.1088/1674-1137/38/5/056001>.
- [10] F. Bečvář, J. Čížek, I. Procházka, J. Janotová, The asset of ultra-fast digitizers for positron-lifetime spectroscopy, *Nucl. Instrum. Methods Phys. Res. A* 539 (1–2) (2005) 372–385, <http://dx.doi.org/10.1016/j.nima.2004.09.031>.
- [11] M. Petriska, A. Zeman, V. Slugeň, V. Kršjak, S. Sojak, L. Debarberis, Application of fast-digitizer card acqiris DP-240 in positron lifetime spectroscopy, *Phys. Status Solidi C* 6 (11) (2009) 2465–2467, <http://dx.doi.org/10.1002/pssc.200982095>, arXiv:<https://onlinelibrary.wiley.com/doi/pdf/10.1002/pssc.200982095>.
- [12] H.B. Wang, Q.H. Zhao, H. Liang, B.C. Gu, J.D. Liu, H.J. Zhang, B.J. Ye, A new SIPM-based positron annihilation lifetime spectrometer using LYSO and LFS-3 scintillators, *Nucl. Instrum. Methods Phys. Res. A* 960 (2020) 163662, <http://dx.doi.org/10.1016/j.nima.2020.163662>.
- [13] F. Bečvář, Digital positron lifetime spectroscopy: present status and outlook, *Phys. Status Solidi (C)* 4 (10) (2007) 3939–3946, <http://dx.doi.org/10.1002/pssc.200675763>.
- [14] D. Petschke, T. Staab, A supervised machine learning approach using naive Gaussian Bayes classification for shape-sensitive detector pulse discrimination in positron annihilation lifetime spectroscopy (PALS), *Nucl. Instrum. Methods Phys. Res. A* 947 (2019) 162742, <http://dx.doi.org/10.1016/j.nima.2019.162742>.
- [15] M. Nelson, B. Rooney, D. Dinwiddie, G. Brunson, Analysis of digital timing methods with baf<sub>2</sub> scintillators, *Nucl. Instrum. Methods Phys. Res. A* 505 (1–2) (2003) 324–327, [http://dx.doi.org/10.1016/s0168-9002\(03\)01078-7](http://dx.doi.org/10.1016/s0168-9002(03)01078-7).
- [16] H. Saito, T. Hyodo, Direct measurement of the parapositronium lifetime in  $\alpha$ -SiO<sub>2</sub>, *Phys. Rev. Lett.* 90 (19) (2003) <http://dx.doi.org/10.1103/physrevlett.90.193401>.
- [17] GNU Scientific Library webpage, URL <http://www.gnu.org/software/gsl/>.
- [18] ROOT webpage, URL <https://root.cern.ch/>.
- [19] Code download page, URL [https://github.com/zqh0053/PALS\\_offline\\_lecroy](https://github.com/zqh0053/PALS_offline_lecroy).
- [20] WIKI webpage, URL [https://en.wikipedia.org/wiki/Spline\\_interpolation](https://en.wikipedia.org/wiki/Spline_interpolation).
- [21] D. Petschke, T.E. Staab, Update (v1.3) to dltPulseGenerator: A library for the simulation of lifetime spectra based on detector-output pulses, *SoftwareX* 9 (2019) 183–186, <http://dx.doi.org/10.1016/j.softx.2019.02.003>, URL <https://www.sciencedirect.com/science/article/pii/S235271101930038X>.
- [22] D. Petschke, T.E. Staab, Ddrs4pals: A software for the acquisition and simulation of lifetime spectra using the DRS4 evaluation board, *SoftwareX* 10 (2019) 100261, <http://dx.doi.org/10.1016/j.softx.2019.100261>, URL <https://www.sciencedirect.com/science/article/pii/S2352711019300676>.
- [23] P.S. oes, J.D. Santos, C. Conde, Gas proportional scintillation counter pulse-signature analysis using digital techniques, *Nucl. Instrum. Methods Phys. Res. A* 422 (1) (1999) 341–346, [http://dx.doi.org/10.1016/S0168-9002\(98\)00978-4](http://dx.doi.org/10.1016/S0168-9002(98)00978-4).
- [24] X. Guo, Z. Wang, Effect of niobia on the defect structure of yttria-stabilized zirconia, *J. Eur. Ceram. Soc.* 18 (3) (1998) 237–240, [http://dx.doi.org/10.1016/s0955-2219\(97\)00123-4](http://dx.doi.org/10.1016/s0955-2219(97)00123-4).
- [25] O. Melikhova, J. Kuriplach, J. Čížek, W.A. I. Procházka, G. Brauer, T. Konstantinova, I. Danilenko, Positron annihilation in three zirconia polymorphs, *Phys. Status Solidi (C)* 4 (10) (2007) 3831–3834, <http://dx.doi.org/10.1002/pssc.200675858>.

- [26] J. Kansa, Microcomputer program for analysis of positron annihilation lifetime spectra, *Nucl. Instrum. Methods Phys. Res. A* 374 (2) (1996) 235–244, [http://dx.doi.org/10.1016/0168-9002\(96\)00075-7](http://dx.doi.org/10.1016/0168-9002(96)00075-7), URL <https://www.sciencedirect.com/science/article/pii/0168900296000757>.
- [27] J. Olsen, P. Kirkegaard, N. Pedersen, M. Eldrup, PALSfit: A New program for the evaluation of positron lifetime spectra, *Phys. Status Solidi (C)* 4 (10) (2007) 4004–4006, <http://dx.doi.org/10.1002/pssc.200675868>.
- [28] J.V. Olsen, P. Kirkegaard, N.J. Pedersen, M. Eldrup, Palsfit: A new program for the evaluation of positron lifetime spectra, *Phys. Status Solidi C* 4 (10) (2007) 4004–4006, <http://dx.doi.org/10.1002/pssc.200675868>, arXiv:<https://onlinelibrary.wiley.com/doi/pdf/10.1002/pssc.200675868>.
- [29] N. Djourelov, M. Misheva, Source correction in positron annihilation lifetime spectroscopy, *J. Phys.: Condens. Matter* 8 (12) (1996) 2081–2087, <http://dx.doi.org/10.1088/0953-8984/8/12/020>.
- [30] G. Kanda, L. Ravelli, B. Loewe, W. Egger, D. Keeble, Positron annihilation lifetime spectroscopy study of kapton thin foils, *J. Phys. D: Appl. Phys.* 49 (2) (2015) 025305, <http://dx.doi.org/10.1088/0022-3727/49/2/025305>.